J Neuropathol Exp Neurol
Vol. 75, No. 4, April 2016, pp. 358–365
doi: 10.1093/jnen/nlw007

ORIGINAL ARTICLE

Malignant Transformation of a Dysembryoplastic Neuroepithelial Tumor (DNET) Characterized by Genome-Wide Methylation Analysis

Dieter Henrik Heiland, MD, Ori Staszewski, MD, Martin Hirsch, MD, Waseem Masalha, MD, Pamela Franco, MD, Jürgen Grauvogel, MD, David Capper, MD, Daniel Schrimpf, Dr. sci. hum., Horst Urbach, MD, and Astrid Weyerbrock, MD

Abstract

Dysembryoplastic neuroepithelial tumors (DNET) are considered to be rare, benign, and associated with chronic epilepsy. We present the case of a 28-year-old man with a history of epilepsy since age 12. Surgery of an occipital cortical lesion in 2009 revealed a DNET. Five years later, a recurrent tumor at the edge of the resection cavity was removed, and the tissue underwent an intensive diagnostic workup. The first tumor was unequivocally characterized as a DNET, but neuropathological diagnostics of the recurrent tumor revealed a glioblastoma. After 6 months, another recurrent tumor was detected next to the location of the original tumor, and this was also resected. An Illumina 450 K beadchip methylation array was performed to characterize all of the tumors. The methylation profile of these tumors significantly differed from other glioblastoma and epilepsy-associated tumor profiles and revealed a DNET-like methylation profile. Thus, molecular characterization of these recurrent tumors suggests malignant transformation of a previously benign DNET. We found increased copy number changes in the recurrent DNET tumors after malignant transformation. Modern high-throughput analysis adds essential molecular information in addition to standard histopathology for proper identification of rare brain tumors that present with an unusual clinical course.

Key Words: Copy number changes, Dysembryoplastic neuroepithelial tumor (DNET), Epigenetic alteration, Illumina 450 K beadchip methylation array, Malignant DNET, Methylation.

INTRODUCTION

Dysembryoplastic neuroepithelial tumors (DNETs) are classified as low-grade (World Health Organization [WHO] I) tumors with a good prognosis. If they are symptomatic, they can be treated successfully by surgery alone. Daumas-Duport et al first described DNETs as curable tumors of young patients; they are cortical lesions with multinodular architecture containing loci resembling diffuse oligodendroglioma, oligoastrocytoma, and astrocytoma elements with "floating neurons" (1). Kleihues et al described DNETs as slow-growing tumors that typically do not undergo malignant transformation to high-grade tumors (2). Moreover, 11 cases of suspected recurrent DNET were recently reanalyzed and reclassified as low- or high-grade astrocytoma or oligoastrocytoma based on histopathological and immunohistochemical features (3). Malignant transformation of DNET is not considered in the current version of the WHO classification of CNS tumors, and no information exists whether or not these tumors maintain their DNET characteristics upon malignant transformation. We report the case of a recurrent DNET with secondary malignant transformation mimicking histopathological features of a glioblastoma (GBM). Methylation analysis by Illumina 450 K beadchip methylation array and comparison with methylation patterns of glial tumors in The Cancer Genome Atlas and the German Cancer Research Center (DKFZ) databases allowed identification of the recurrent tumor as a DNET that had undergone malignant transformation with a methylation pattern distinct from that of malignant gliomas.

MATERIALS AND METHODS

Patient

A 28-year-old man suffered from a seizure disorder since the age of 12. His disorder was described as structural epilepsy with visual aura followed by secondary bilateral tonic-clonic seizures. In 2009, an MRI brain scan revealed a cortical and subcortical occipital lesion localized next to the optical fiber tracts with low signal in T1-weighted images, high signal in T2-weighted images, and no contrast enhancement or mass effect (Fig. 1A). The tumor was identified as the epileptogenic focus by presurgical epilepsy diagnostics.

From the Department of Neurosurgery (DHH, WM, PF, JG, AW), Department of Pathology, Institute of Neuropathology (OS), Department of Neurosurgery, Epilepsy Center (MH), and Department of Neuroradiology (HU), Medical Center - University of Freiburg, Freiburg, Germany; and Department of Neuropathology, University Heidelberg, Im Neuenheimer Feld 224 and German Cancer Consortium (DKTK), CCU Neuropathology, German Cancer Research Center (DKFZ), Heidelberg, Germany (DC, DS).

Send correspondence to: Astrid Weyerbrock, MD, Department of Neurosurgery, Medical Center - University of Freiburg, Breisacher Strasse 64, 79106 Freiburg, Germany; E-mail: astrid.weyerbrock@uniklinik-freiburg.de

This study was supported by the core facility of CCU Neuropathology, German Cancer Research Center, Heidelberg, Germany.

The patient underwent surgery, and the tumor was subtotally resected due to the proximity to the optic tract, which was successfully preserved. Histopathologically, the tumor was characterized as a DNET WHO grade I (Fig. 2). Yearly postoperative follow-up scans were performed (Fig. 1B, C). Five years later, the patient developed deterioration of his overall clinical condition and an increase in the frequency of the epileptic seizures. An MRI brain scan revealed a new contrast-enhancing lesion with slight mass effect but without extensive brain edema next to the cortical left occipital resection

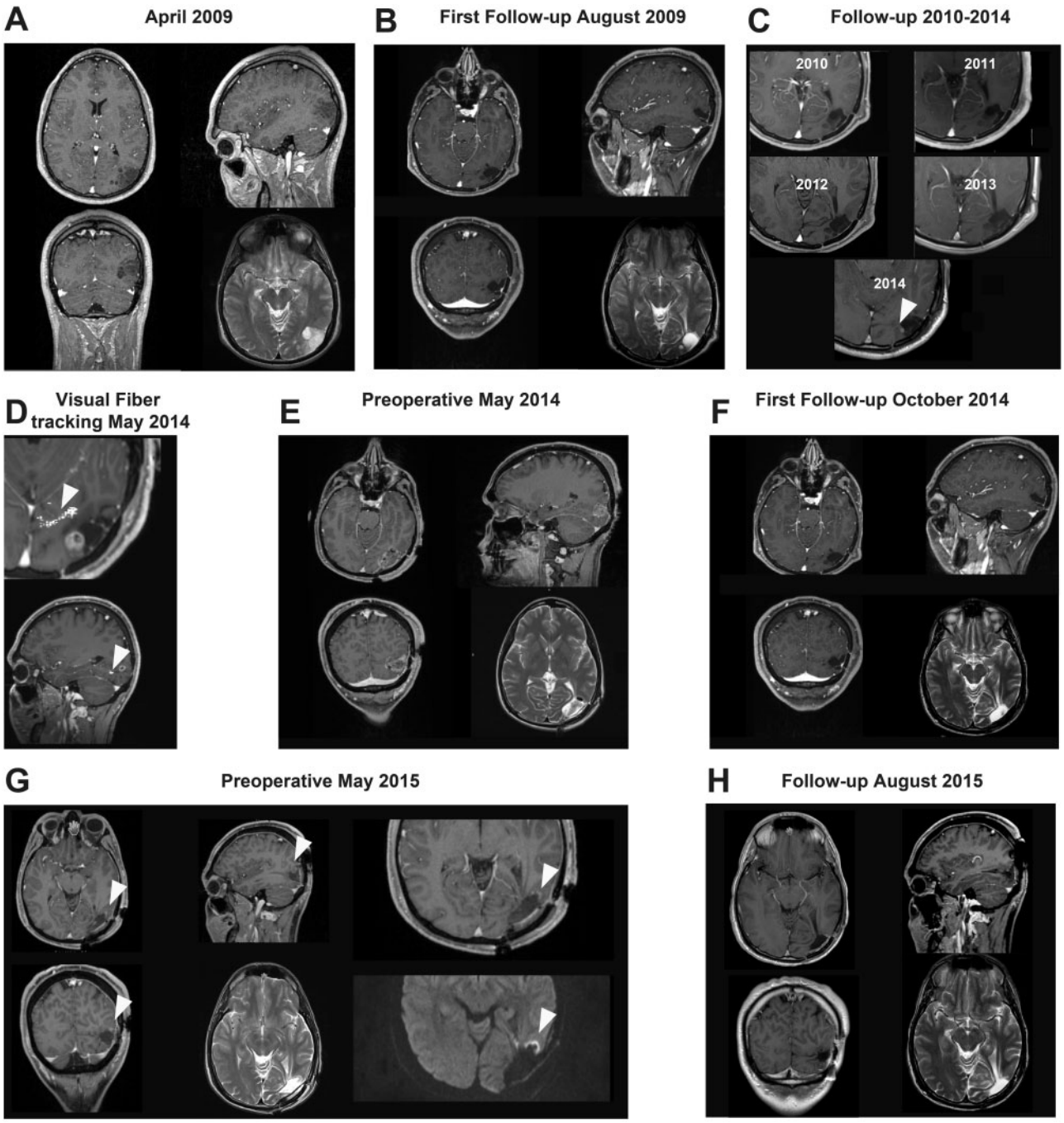

FIGURE 1. (A, B) Pre- and postoperative MRIs from 2009; T1-weighted images with contrast enhancement and T2-weighted images. **(C)** Follow-up MRIs from 2010 until tumor progression in 2014. **(D)** Preoperative tractography of the visual tracts. The tractography is superimposed on the MRI using white dots and marked with an arrow. **(E)** Preoperative T1-weighted images with contrast enhancement and T2-weighted images. **(F)** T1- and T2-weighted images of the first follow-up in 2014. **(G)** Preoperative T1-weighted images with contrast enhancement (arrow) and T2-weighted and diffusion images, May 2015 (arrowheads). **(H)** Postoperative MRIs from 2015: T1-weighted images with contrast enhancement and T2-weighted images.

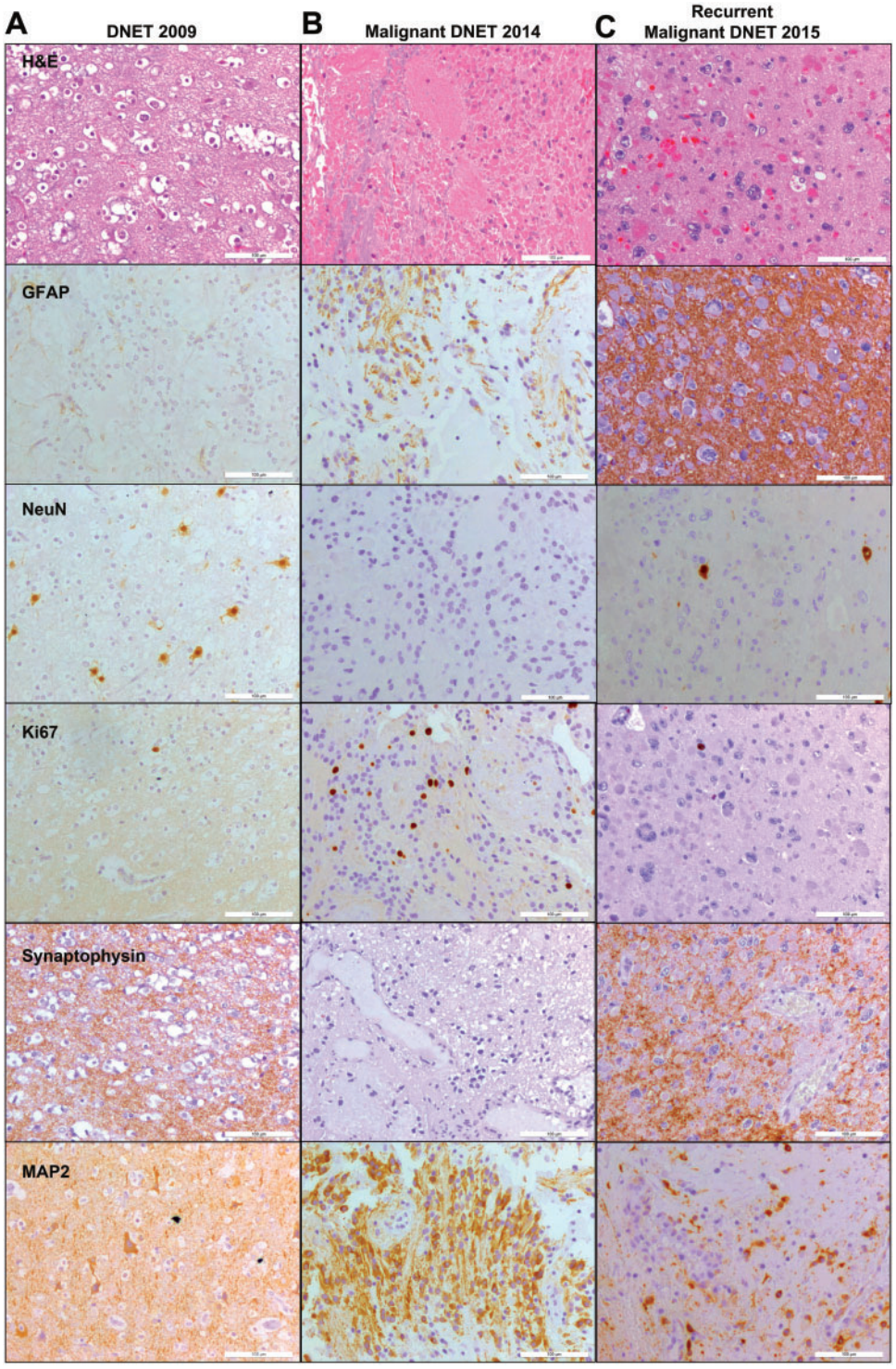

FIGURE 2. Histopathology and immunostaining of samples in 2009, 2014, and 2015. **(A)** In 2009, hematoxylin and eosin (H&E) staining shows loss of oligodendroglia-like cells. The tumor of 2009 shows typical dysembryoplastic neuroepithelial tumor (DNET) morphology. **(B)** In the recurrent tumor (2014), microtubule-associated protein 2 (Map2) immunohistochemistry stains some tumor cells with prominent cellular processes; no neurons are stained. Ki67 immunostaining reveals a strongly increased proliferative activity with about 10% of cells staining positively in 2014 compared with <1% in 2009 **(A)**. The histological and immunohistochemical findings of the recurrent tumor bear all hallmarks of a glioblastoma (WHO IV). **(C)** The histological and immunohistochemical findings of the recurrent malignant DNET show parts of GBM morphology but also DNET features. GFAP, glial fibrillary acidic protein.

cavity. A preoperative MRI scan with tractography of the visual tracts was obtained for intraoperative navigation (Fig. 1D, E). The tumor was removed, and a comprehensive diagnostic and molecular analysis was performed. The patient underwent postoperative adjuvant radiotherapy. The 3-month follow-up scan showed no tumor progression (Fig. 1F). Six months after the surgery, new contrast enhancing lesions were detected around the resection cavity (Fig. 1G). Again, the tumor was removed, and intensive comprehensive diagnostic and molecular analysis was performed. The most recent 3-month follow-up in August 2015 showed no tumor progression (Fig. 1H).

Histopathological and Immunohistochemical Analyses

Standard histology was performed on paraffin-embedded tumor tissue after written informed consent of the patient. Retrieval and scientific analysis of patient-derived tissue was approved by the local ethics committee under protocol 100020/09.

Tissue samples were fixed using 4% phosphate-buffered formaldehyde and paraffin embedded with standard procedures. Hematoxylin and eosin stains were performed on 4-μm paraffin sections using standard protocols. Immunohistochemistry was performed using an autostainer (Dako, Glostrup, Denmark) after heat-induced epitope retrieval in citrate buffer. Primary antibodies used were to glial fibrillary acidic protein ([GFAP] 1:1000, Zytomed Systems, Berlin, Germany), NeuN (1:500, Millipore, Billerica, MA), Ki-67 (Mib1, 1:50, Dako), microtubule-associated protein 2 ([Map2] 1:10,000, Sigma-Aldrich, St Louis, MO), and synaptophysin (1:50, Dako). Diaminobenzidine DAB staining was performed using the Envision Flex High pH Kit (Dako). Isocitrate dehydrogenase IDH1 mutation was assessed by immunohistochemistry using an anti-IDH1-R123 antibody (1:20, Dianova, Hamburg, Germany).

Methylation Analysis

DNA was extracted from tumor tissue and underwent methylation analysis using the Infinium HumanMethylation450 BeadChip array (www.illumina.com) at the DKFZ core facility (Heidelberg, Germany). All raw data of the Illumina 450 K beadchip methylation array were analyzed with R-software and available packages (www.biocoductor.com). Data were imported and analyzed using the RnBeads pipeline (http//:rnbeads.mpi-inf.mpg.de). Quality control was done by major quality-control algorithms, including sample-independent controls. In a preprocessing Greedycut, 4713 CpG sites were removed because they overlap with single nucleotide polymorphisms and cause unreliable measurements. The background subtraction was performed using the methylumi package. We used the Beta-Mixture Quantile Normalization (BMIQ) method to normalize β-methylation values. In addition, we removed sex chromosomal probes (n = 11,497). Methylation profiles were computed for the specific gene region types as whole gene regions, promoter region, and individual CpG islands. Differential methylation on gene regions was computed by *t*-test-based statistics (paired *t* test with false discovery rate (FDR)-adjusted p value) in the limma r-tool. Data visualization was done in ggplot2 (r-based). Methylation data of the DNET and malignant DNETs were added to the DKFZ database and clustered by average-based unsupervised hierarchical cluster (Euclidean distance, complete linkage).

Analysis of DKFZ Tumor Samples

Tumor samples (n = 116) from the DKFZ tumor database were used as reference samples. For further cluster analysis, we included 44 patients with a GBM. Fifteen out of 44 were classified as an H3.3 K27-mutated GBM; 14 patients had a G34 mutation. Methylation profiling grouped 15 patients into the receptor tyrosine kinase (RTK) I subgroup and 14 patients into the GBM classic (RTK II) subgroup. Fifteen patients had a R132H-mutated astrocytoma with a glioma CpG methylated phenotype (G-CIMP)-positive methylation pattern. In addition, typical epilepsy-associated tumors, including ganglioglioma (n = 13), DNET (n = 14), and pleomorphic xanthoastrocytoma (PXA) (n = 15), were included in the cluster analysis. Raw data were processed as described above including agglomerative hierarchical clustering (median based). The clustering was performed at the DKFZ (Heidelberg, Germany).

Copy Number Profile

A copy number profile was done by R-software included in the conumee package (4) (www.biocoductor.com). This tool allows performing copy number variation analysis on Infinium HumanMethylation450 BeadChip data. This function of detecting copy number alterations in HumanMethylation450 data was first described by Feber et al (5). Sturm et al used this tool to detect specific chromosomal aberrations in cancer samples (6). Copy number variation analysis was performed in a 2-step approach by combining methylated and unmethylated intensity values of each CpG probe and normalizing them with normal brain controls. In the next step, neighboring probes were combined by hybridization method. Finally, segmentation was performed by circular binary segmentation algorithm implemented in the DNAcopy package (5). Visualization included in the conumee package was performed at the DKFZ (Heidelberg, Germany).

RESULTS

Histopathology and Immunohistochemistry

Hematoxylin-and-eosin-stained tissue sections obtained from the primary tumor in 2009 showed CNS tissue with sheaths and isolated nodules of monomorphic cells within a relatively sparse microcystic matrix. The tumor cells exhibited oligodendroglia-like morphology with monomorphic, small, round nuclei and optically clear perinuclear halos (Fig. 2A). Scattered isolated neurons were detected in NeuN immunostains. Synaptophysin immunohistochemistry showed a positively stained tumor matrix. Immunohistochemical staining for GFAP revealed weak GFAP-positive staining of the matrix with some activated astrocytes interspersed between the tumor cells; the tumor cells showed no GFAP expression. The scattered neurons were also

stained positively for Map2. The proliferation, marked by Ki-67, was below 1% (Fig. 2A).

In contrast to the primary lesion resected in 2009, the recurrent tumor in 2014 exhibited glial appearance with a lack of perinuclear halos and comparatively pleomorphic nuclei (Fig. 2B). The cell density was increased with areas of necrosis and microvascular proliferation. GFAP and Map2 immunostaining revealed fibrillary staining for GFAP in some tumor cells and strong staining for Map2. Notably, neuronal structures were absent, and NeuN and synaptophysin staining were negative. In the Ki67 immunostaining, positive staining of approximately 10% of the cells indicated increased tumor-cell proliferation. The histological and immunohistochemical findings of the recurrent tumor bear all hallmarks of GBM, WHO IV with an astroglial (GFAP-positive) component, necrosis, and microvascular proliferation. In addition, R123H-IDH1 mutation could be not detected in the original and recurrent DNET by immunostaining or Illumina 450 K beadchip methylation array (data not shown). The Illumina 450 K beadchip methylation array is a powerful tool to identify the IDH mutation by its epigenetic changes (G-CIMP) (7). Therefore, additional IDH-1 or IDH-2 sequencing was not necessary. The histological specimens were sent to 2 neuropathological reference centers (Heidelberg and Bonn, Germany) to obtain second opinions; both confirmed the histological features of a malignant glioma. The 1p19q-codeletion status was assessed by Illumina 450 K beadchip methylation array and additional copy number variation analysis. There were no typical gain and loss of 1p or 19q detected in the primary or recurrent tumors.

The second recurrent malignant DNET showed a similar histological appearance as the first malignant DNET (Fig. 2C). Scattered neuronal structures were detected by NeuN staining, showing isolated neurons, and antisynaptophysin staining, showing positive reaction in parts of the tumor matrix. Increases of necrotic regions and nuclear pleomorphism were detected in the tumor. The second tumor–recurrence tumor showed monomorphic cells within a relatively sparse microcystic matrix and areas of necrosis and microvascular proliferation. GFAP and Map2 immunostainings revealed strong fibrillary staining for GFAP and expression of Map2 in some of the tumor cells (Fig. 2C). In addition, the second recurrent malignant DNET was partly heterogeneous with parts of typical GBM morphology but also some areas of DNET morphology.

Methylation Analysis Identifies Different Methylation Patterns

Methylation data of the DNET samples (primary and 2 recurrences), GBM from the The Cancer Genome Atlas database (subgrouped in GBM-K27, GBM-G34, GBM-RTK-I, and GBM-RTK-II-Classical), and other epilepsy-associated tumors (ie, PXA and ganglioglioma) were clustered by Euclidean distance. The cluster analysis clearly showed distinct methylation patterns of the DNET WHO grade I and the malignant DNETs compared with GBM samples or other epilepsy-associated tumor types (Fig. 3A). Analysis of the original and the malignant DNET tumor revealed several genes with methylation changes: 865 hypomethylated (>0.2 methylation difference) and 76 hypermethylated genes in the malignant DNET (>0.2 methylation difference) (Fig. 3B). Genes that are strongly demethylated in the malignant DNET included *TRDD2* and *TRDJ1*, 2 genes that play a role in T-cell receptor binding, and *IGHVIII-44*, which is associated with the immune system. On the other hand, we found a loss of gene promoter methylation of oncogenes such as *HULC*, which is linked to hepatocellular cancer (8). Further analysis showed a genome-wide distribution of the methylation differences (Fig. 3C, D). These methylation patterns are only partially associated with copy number changes. In summary, there was a loss of methylation after malignant transformation resulting in a methylation pattern distinct from the typical pattern of the GBM samples (Fig. 3A). Most of the methylation changes were on chromosomes 1, 6, and 15. A detailed analysis of methylation changes in specific gene regions could not be performed ($n=1$).

Multiple chromosomal aberrations were seen after malignant transformation. As shown in Fig. 4A, typical DNETs do not have any chromosomal aberrations. As expected, the copy number profile of the original DNET did not reveal any chromosomal aberrations. After malignant transformation, losses on chromosome 10, 14–19, and 22 were detected (Fig. 4B). Only chromosome 21 revealed a slight gain. In the recurrent malignant DNET, the chromosomal aberrations increased (Fig. 4C). Copy number changes were detected with a gain on chromosomes 5–7 and 21. A chromosomal loss was found on chromosomes 2, 9–11, 13–14, 16, 19, and 22 (Fig. 4C).

DISCUSSION

Here, we describe for the first time the malignant transformation of an initially benign DNET (confirmed by modern high-throughput analysis), the recurrence of which was initially classified as a malignant glioma based on standard neuropathological diagnostics. We introduce an Illumina 450 K beadchip methylation array as a diagnostic tool to characterize brain tumors and identify differences in their methylation profiles. The Illumina 450 K beadchip methylation array is widely used in research to analyze genome-wide methylation changes, for example, in IDH-mutated gliomas (9). A recent study showed different GBM subtypes that could be identified by methylation array (6). By unsupervised clustering of these GBM subtypes and other epilepsy-associated tumors, we identified individually clustered subgroups. Specific methylation profiles were representative for each tumor entity. This technique is new and not well established but adds valuable additional information to classic histopathological findings.

Malignant transformation of a DNET is a rare phenomenon with few cases described in the literature; at this time, this is not considered in the WHO classification of tumors of the CNS (10). A recent literature review of malignant DNET cases identified 11 cases of malignant transformation of tumors primarily categorized as WHO grade I DNET. The recurrent tumors were most often classified as oligo- or astrocytomas ranging from grades II to IV or pilocytic astrocytomas. We report the transformation of a DNET WHO grade I into a "high-grade DNET." Its methylation

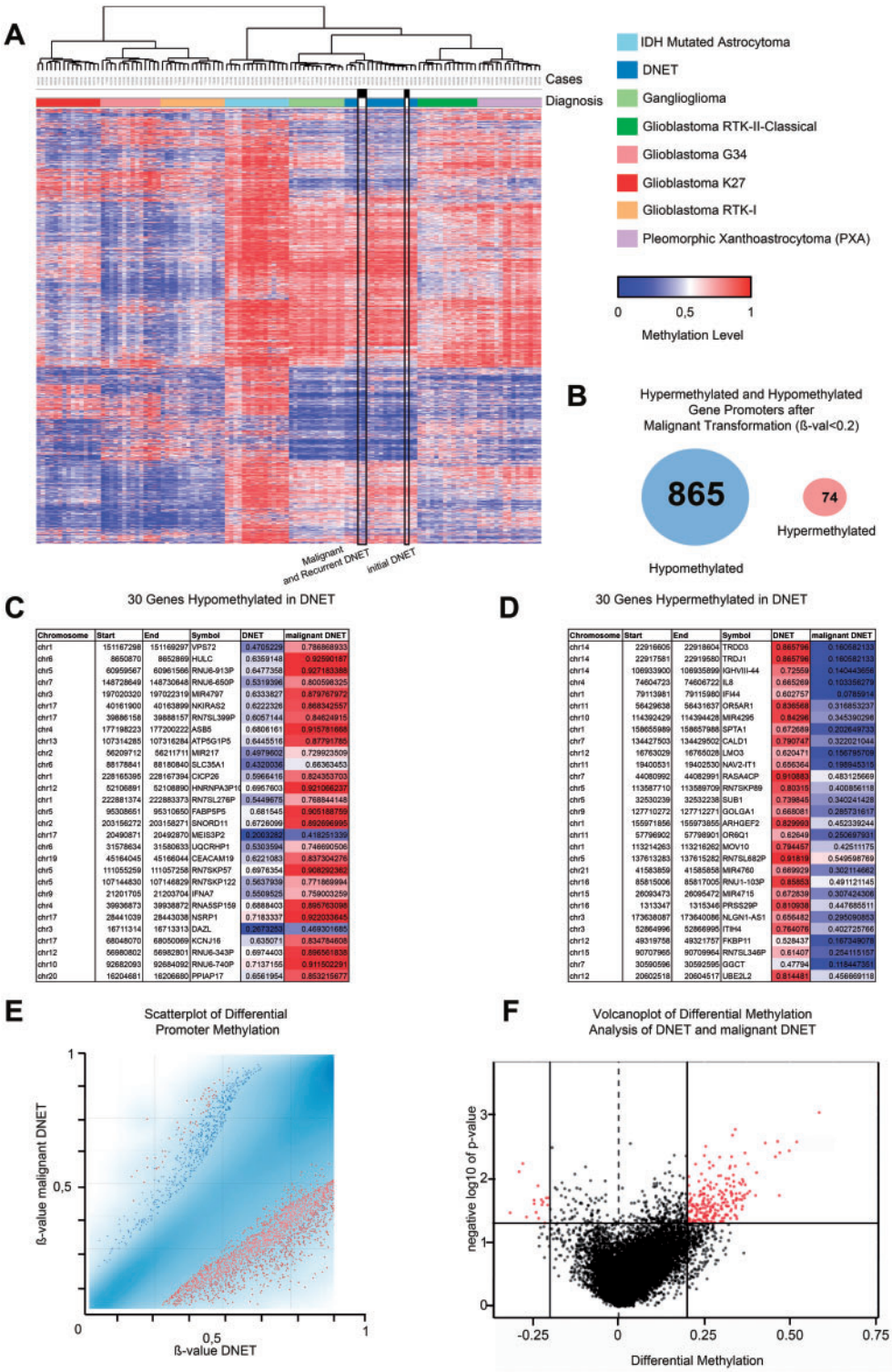

Chromosome	Start	End	Symbol	DNET	malignant DNET
chr1	151167298	151169297	VPS72	0.4705228	0.788868933
chr6	8650870	8652869	HULC	0.6358148	0.92590157
chr5	60959567	60961566	RNU6-913P	0.6477358	0.927183388
chr7	148728649	148730648	RNU6-650P	0.5319396	0.800598325
chr3	197020320	197022319	MIR4797	0.6333827	0.879767972
chr17	40161900	40163899	NKIRAS2	0.6222326	0.868342557
chr17	39886158	39888157	RN7SL399P	0.6057144	0.84624915
chr4	177198223	177200222	ASB5	0.6806161	0.915781668
chr13	107314285	107316284	ATP5G1P5	0.6445516	0.87791785
chr2	56209712	56211711	MIR217	0.4979602	0.729923509
chr6	88178841	88180840	SLC35A1	0.4320036	0.66363453
chr1	228165395	228167394	CICP26	0.5966416	0.824353703
chr12	52106891	52108890	HNRNPA3P10	0.6957603	0.921066237
chr1	222861374	222883373	RN7SL276P	0.5449675	0.768844148
chr5	95308661	95310660	FABP5P5	0.681545	0.955189756
chr2	203156272	203158271	SNORD11	0.6726099	0.892696995
chr17	20490871	20492870	MEIS3P2	0.2003282	0.418251339
chr6	31578634	31580633	UQCRHP1	0.5303594	0.746690506
chr19	45164045	45166044	CEACAM19	0.6221083	0.837304276
chr5	111055259	111057258	RN7SKP57	0.6976354	0.908292362
chr5	107144830	107146829	RN7SKP122	0.5637939	0.771869994
chr9	21201705	21203704	IFNA7	0.5509525	0.759003259
chr4	39936873	39938872	RNA5SP159	0.6888403	0.895763096
chr17	28441039	28443038	NSRP1	0.7183337	0.922033645
chr3	16711314	16713313	DAZL	0.2673253	0.489301685
chr17	68048070	68050069	KCNJ16	0.635071	0.834784608
chr12	56982802	56982801	RNU6-343P	0.6974403	0.896561838
chr10	92682093	92684092	RNU6-740P	0.7137155	0.911522291
chr20	16204681	16206680	PPIAP17	0.6561954	0.853215677

Chromosome	Start	End	Symbol	DNET	malignant DNET
chr14	22918605	22918604	TRDD3	0.865796	0.160582133
chr14	22917581	22919580	TRDJ1	0.865796	0.160582133
chr14	106933900	106935899	IGHV3II-44	0.72559	0.140443656
chr4	74604723	74606722	IL8	0.665269	0.103356279
chr1	79113981	79115980	IFI44	0.602757	0.0785914
chr11	56429638	56431637	OR5AR1	0.836569	0.316853237
chr10	114392429	114394428	MIR4295	0.84296	0.345390298
chr1	158655989	158657988	SPTA1	0.672689	0.202649733
chr7	134427503	134429502	CALD1	0.790747	0.322021044
chr12	16763029	16765028	LMO3	0.620471	0.156795709
chr11	19400531	19402530	NAV2-IT1	0.656364	0.198845316
chr7	44080992	44082991	RASA4CP	0.910883	0.483125669
chr5	113587710	113589709	RN7SKP89	0.89315	0.400856118
chr5	32530237	32532236	SUB1	0.739645	0.340241428
chr9	127710272	127712271	GOLGA1	0.668061	0.285731617
chr1	155971856	155973855	ARHGEF2	0.829993	0.452339244
chr11	57796902	57798901	OR8Q1	0.62649	0.250697931
chr1	113214263	113216262	MOV10	0.794457	0.42511175
chr5	137613283	137615282	RN7SL682P	0.91819	0.549598769
chr21	41583859	41585858	MIR4760	0.669929	0.302114662
chr16	85815006	85817005	RNU1-103P	0.85853	0.491121145
chr15	26093473	26095472	MIR4715	0.672839	0.307424306
chr16	1313347	1315346	PRSS29P	0.810938	0.447685511
chr3	173638087	173640086	NLGN1-AS1	0.656482	0.295090853
chr3	52864996	52866995	ITIH4	0.764076	0.402725766
chr12	49319758	49321757	FKBP11	0.528437	0.167349079
chr15	90707955	90709954	RN7SL346P	0.61407	0.254115107
chr7	30590596	30592595	GGCT	0.47794	0.115447351
chr12	20602518	20604517	UBE2L2	0.814481	0.456869118

FIGURE 3. (A) Hierarchical cluster of different glioblastoma subtypes (G43, RTK-I, RTK-II, K27, IDH1-mutated) and other epilepsy-associated tumors (ganglioglioma, dysembryoplastic neuroepithelial tumor [DNET], PXA). The heatmap shows the 1000 most-variable CpG sites with low methylation values colored in blue, medium methylation level in white, and high methylation CpG in red. Samples of the origin DNET and the recurrent tumors are marked in black. **(B)** After malignant transformation of the original DNET, 754 gene promoters were strongly demethylated (mean methylation changes of CpG sites in gene promoter, $p > 0.2$); 74 showed increased methylation ($p > 0.2$). **(C, D)** Differential methylation of genes in DNET before and after malignant transformation. **(E, F)** Volcano and scatter plots of differential methylation of gene promoters.

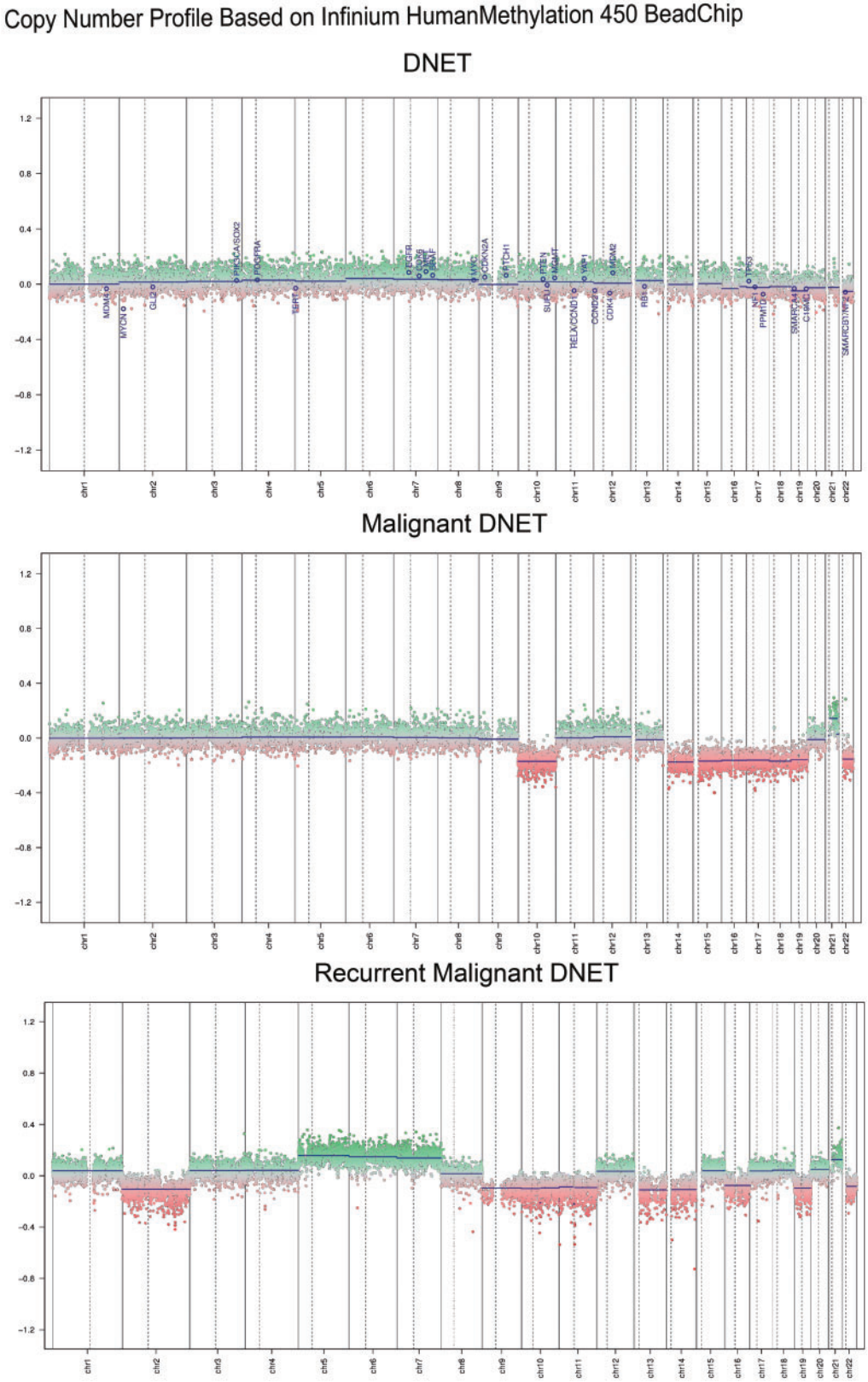

FIGURE 4. Copy number variants (CNV) of the origin dysembryoplastic neuroepithelial tumor (DNET) and the recurrent tumors of 2014 and 2015. Increased numbers of CNVs with gene loss and gain were detected after malignant transformation. **(A)** Original DNET. **(B)** DNET after malignant transformation. **(C)** Recurrent malignant DNET.

pattern clearly differs from typical glioma methylation patterns that have been described (6, 11, 12). In particular, all specific GBM methylation subgroups were clearly distinct from the DNET and malignant DNET methylation patterns. Therefore, despite histological criteria of a malignant glioma (ie, staining for glial markers, high proliferation, necrosis, and angiogenesis), the recurrent tumor should be categorized as a malignant DNET with reference to its tumor of origin and the methylation pattern incompatible with established methylation patterns of GBM subtypes. Comparison of the methylation patterns of the original and recurrent malignant DNET indicates a loss of methylation of a variety of promoter regions after malignant transformation. These methylation changes lead to the massive chromosomal aberrations shown in Fig. 4. We performed differential methylation analysis to identify genes that potentially could play a role in the malignant transformation. On the basis of an individual case, further specific methylation and pathway analysis is not possible. Because of the low sample number of DNETs (n = 13) and malignant DNETs (n = 2 [of the same patient]), the results of this analysis are of interest but have low explanatory power. We found increased methylation in genes associated with the T-cell response and the immune system, whereas oncogenes such as *HULC* were demethylated (8). Another demethylated gene was *VPS72*, a gene that plays a role in hematopoietic stem cell development (13). These findings must be verified in a larger sample of malignant DNETs. In addition, we saw a gain on chromosome 21 and several chromosomal losses. These chromosomal aberrations are common in a variety of leukemias and thyroid cancers (14) and require further analysis of their biological relevance. Interestingly, chromosomal aberrations and instability were never described in DNET, whereas malignant gliomas show massive instabilities (15, 16). The recurrence of the malignant DNET emphasized its aggressive phenotype. We detected an increased number of chromosomal aberrations in the second recurrent malignant DNET, which represent an ongoing malignant transformation.

Although our analysis includes 1 case of primary and malignant transformed DNET, it clearly points to the increasing importance of high-throughput molecular analysis of CNS tumors for proper identification of rare tumors with distinct marker profiles and unusual clinical courses. These results have to be reevaluated with more matched tumor samples of transformed tumors.

This study describes for the first time the molecular subtype of a malignant DNET identified by Illumina 450 K beadchip methylation array. Adding molecular data to standard neuropathological analysis allows proper identification of rare CNS tumors and identification of specific subtypes based on the pattern of molecular markers and may help delivering the adequate treatment to the affected patients.

REFERENCES

1. Daumas-Duport C, Scheithauer BW, Chodkiewicz JP, et al. Dysembryoplastic neuroepithelial tumor: A surgically curable tumor of young patients with intractable partial seizures. Report of thirty-nine cases. Neurosurgery 1988;23:545–56
2. Kleihues P, Burger PC, Scheithauer BW. The new WHO classification of brain tumours. Brain Pathol 1993;3:255–68
3. Moazzam AA, Wagle N, Shiroishi MS. Malignant transformation of DNETs: A case report and literature review. Neuroreport 2014;25:894–9
4. Hovestadt V, Zapatka M. Conumee: Enhanced copy-number variation analysis using Illumina 450k methylation arrays. Available at: https://www.bioconductor.org/packages/release/bioc/html/conumee.html
5. Feber A, Guilhamon P, Lechner M, et al. Using high-density DNA methylation arrays to profile copy number alterations. Genome Biol 2014;15:R30
6. Sturm D, Witt H, Hovestadt V, et al. Hotspot mutations in H3F3A and IDH1 define distinct epigenetic and biological subgroups of glioblastoma. Cancer Cell 2012;22:425–37
7. Wiestler B, Capper D, Hovestadt V, et al. Assessing CpG island methylator phenotype, 1p/19q codeletion, and MGMT promoter methylation from epigenome-wide data in the biomarker cohort of the NOA-04 trial. Neuro Oncol 2014;16:1630–8
8. Peng W, Gao W, Feng J. Long noncoding RNA HULC is a novel biomarker of poor prognosis in patients with pancreatic cancer. Med Oncol 2014;31:346
9. Noushmehr H, Weisenberger DJ, Diefes K, et al. Identification of a CpG island methylator phenotype that defines a distinct subgroup of glioma. Cancer Cell 2010;17:510–22
10. Louis DN, Ohgaki H, Wiestler OD, et al. The 2007 WHO classification of tumours of the central nervous system. Acta Neuropathol 2007;114:97–109
11. Verhaak RG, Hoadley KA, Purdom E, et al. Integrated genomic analysis identifies clinically relevant subtypes of glioblastoma characterized by abnormalities in PDGFRA, IDH1, EGFR, and NF1. Cancer Cell 2010;17:98–110
12. Wagner DE, Ho JJ, Reddien PW. Genetic regulators of a pluripotent adult stem cell system in planarians identified by RNAi and clonal analysis. Cell Stem Cell 2012;10:299–311
13. Umemoto T, Yamato M, Ishihara J, et al. Integrin-αvβ3 regulates thrombopoietin-mediated maintenance of hematopoietic stem cells. Blood 2012;119:83–94
14. Fröhling S, Döhner H. Chromosomal abnormalities in cancer. N Engl J Med 2008;359:722–34
15. Brat DJ, Verhaak RG, Cancer Genome Atlas Research Network, et al. Comprehensive, integrative genomic analysis of diffuse lower-grade gliomas. N Engl J Med 2015;372:2481–98
16. Brennan CW, Verhaak RG, McKenna A, et al. The somatic genomic landscape of glioblastoma. Cell 2013;155:462–77